Biochimica et Biophysica Acta 1838 (2014) 3212–3219

Contents lists available at ScienceDirect

Biochimica et Biophysica Acta

journal homepage: www.elsevier.com/locate/bbamem

Residue specific partitioning of KL_4 into phospholipid bilayers

Austin L. Turner [a], Otonye Braide [a], Frank D. Mills [b], Gail E. Fanucci [a,1], Joanna R. Long [b,*]

[a] Department of Chemistry, University of Florida, Gainesville, FL 32611, USA
[b] Department of Biochemistry and Molecular Biology, University of Florida, Gainesville, FL 32610, USA

ARTICLE INFO

Article history:
Received 30 May 2014
Received in revised form 24 August 2014
Accepted 15 September 2014
Available online 22 September 2014

Keywords:
Pulmonary surfactant
KL_4
Power saturation EPR
Membrane-active peptide
Membrane partitioning
Site-directed spin-labeling

ABSTRACT

KL_4, which has demonstrated success in the treatment of respiratory distress, is a synthetic helical, amphipathic peptide mimetic of lung surfactant protein B. The unusual periodicity of charged residues within KL_4 and its relatively high hydrophobicity distinguish it from canonical amphipathic helical peptides. Here we utilized site specific spin labeling of both lipids and the peptide coupled with EPR spectroscopy to discern the effects of KL_4 on lipid dynamics, the residue specific dynamics of hydrophobic regions within KL_4, and the partitioning depths of specific KL_4 residues into the DPPC/POPG and POPC/POPG lipid bilayers under physiologically relevant conditions. KL_4 induces alterations in acyl chain dynamics in a lipid-dependent manner, with the peptide partitioning more deeply into DPPC-rich bilayers. Combined with an earlier NMR study of changes in lipid dynamics on addition of KL_4 (V.C. Antharam et al., 2009), we are able to distinguish how KL_4 affects both collective bilayer motions and intramolecular acyl chain dynamics in a lipid-dependent manner. EPR power saturation results for spin labeled lipids demonstrate that KL_4 also alters the accessibility profiles of paramagnetic colliders in a lipid-dependent manner. Measurements of dynamics and depth parameters for individual spin-labeled residues within KL_4 are consistent with a model where the peptide partitions deeply into the lipid bilayers but lies parallel to the bilayer interface in both lipid environments; the depth of partitioning is dependent on the degree of lipid acyl chain saturation within the bilayer.

1. Introduction

Pulmonary surfactant (PS) is a vital, lipid-rich extracellular fluid that lowers surface tension and provides immunoprotection within the alveoli. PS is comprised of a mixture of phospholipids and proteins, with the major lipid component being 1,2-dipalmitoyl-*sn*-glycero-3-phosphocholine (DPPC). Low concentrations of hydrophobic proteins within PS are critical to its unique physical properties and lipid trafficking functions including the following: facilitating lung expansion at ambient pressure, preventing alveolar collapse, and significantly reducing surface tension in a highly dynamic, organized process [1–3]. Inadequate PS production in premature infants is the leading cause of acute respiratory distress syndrome (ARDS), [4–6] where typical treatment is the administration of exogenous, animal-derived PS via the airways [7,8]. The reliance on these biologically sourced surfactants is due to the difficulty in recombinant expression and purification of the highly hydrophobic surfactant proteins critical to PS function, particularly surfactant protein B (SP-B). Failure to produce functional SP-B leads to respiratory failure and eventual death [9].

Synthetic, peptide-based lung surfactant replacement therapies for RDS therapy have shown promise and can potentially reduce the cost and immunologic risks associated with exogenous animal-derived PS. Functional studies have shown that much of the action of SP-B can be recaptured using peptides 20–25 amino acids in length based on the N- and C-termini of SP-B [10–12]. KL_4, is a 21-mer peptide mimetic of the C-terminus of SP-B, of sequence KLLLLKLLLLKLLLLKLLLLK, and it was designed based on the charge distribution and hydrophobicity of the native protein sequence [13]. KL_4 has demonstrated efficacy for treating ARDS when formulated with palmitic acid and lipids commonly found in PS [14,15]. This formulation, termed Lucinactant, was recently approved for the prevention of RDS in high risk premature infants [16]. Although KL_4 is a promising replacement of SP-B in the treatment for RDS, its mechanism of action remains controversial. The increased effectiveness of KL_4 when compared to other clinically available formulations [17,18] and its greatly simplified amino acid sequence suggest that an understanding of its structural properties and its effects on the molecular and biophysical properties of the lipids could yield fundamental

Abbreviations: PS, pulmonary surfactant; SP-B, surfactant protein B; MLV, multilamellar vesicle; ARDS, acute respiratory distress syndrome; POPC, 1-palmitoyl-2-oleoyl-*sn*-glycero-3-phosphatidylcholine; POPG, 1-palmitoyl-2-oleoyl-*sn*-glycero-3-phosphatidylglycerol; DPPC, 1,2-dipalmitoyl-*sn*-glycero-3-phosphocholine; *n*-doxyl-PSPC, 1-palmitoyl-2-stearoyl-(*n*-doxyl)-*sn*-glycero-3-phosphocholine; P/L, peptide/lipid molar ratio; CD, circular dichroism; FTIR, Fourier transform infrared spectroscopy; SDSL, site-directed spin label; CW-EPR, continuous wave electron paramagnetic resonance; ΔH_{pp}, peak-to-peak linewidth of central resonance line; Bis-Tris, 2-[bis(2-hydroxyethyl)amino]-2-(hydroxymethyl)-1,3-propanediol; NiAA, nickel (II) acetylacetonate; NiEDDA, nickel (II) ethylenediamine-N,N′-diacetic acid; TEMPO-PC, 1-palmitoyl-2-stearoyl-*sn*-glycero-3-phospho(tempo)choline; IAP, iodoacetamido-PROXYL spin label

* Corresponding author. Tel.: +1 352 846 1506.
E-mail address: jrlong@ufl.edu (J.R. Long).
[1] Tel.: +1 352 846 1506.

http://dx.doi.org/10.1016/j.bbamem.2014.09.006
0005-2736/

insights into peptide/lipid interactions for the rational design of novel synthetic mimetics.

Low resolution structural characterization of KL_4 in lipid environments via CD and FTIR has consistently indicated the formation of a helical peptide conformation in lipid suspensions; although some variations in helicity with lipid composition have been reported [19,20]. Experimental characterizations of the orientation of KL_4 have yielded inconsistent, conflicting results. In early FTIR work using DPPC/DPPG (7:3) bilayers, KL_4 was found to be helical and spanning the bilayer in a transmembrane orientation [21]. Later FTIR work, using either DPPC or DPPC/DPPG (7:3) mixtures, indicated that KL_4 lies along the surface of the lipids as a mixture of β-sheet and α-helix at the air/water interface [22]. However, these lower-resolution assays monitored amide I stretching frequencies, which can be solvent dependent [23], and assumed that KL_4 adopts classical β-sheet or α-helix secondary structures. A more recent transcription–translation assay found KL_4 capable of traversing lipid bilayers, suggesting a transmembrane orientation [24]. However, this transcription–translation assay relied on the integration of a DNA sequence encoding KL_4 into the *Escherichia coli* inner membrane protein leader peptidase (Lep) gene, translation of the protein at ER-derived microsomal membranes, and assaying for glycosylation using proteinase K to determine whether the peptide traverses the membrane. This type of host–guest experiment may influence the secondary structure of KL_4 in the lipid bilayers, and KL_4 is known to alter lipid dynamics and trafficking, which may affect the overall integrity of the microsomal membranes.

A possible explanation for these mixed results may lie in a detailed investigation of the exact helical nature of KL_4. Interestingly, the occurrence of lysines at every *fifth* residue in KL_4 prevents a simple amphipathic helical wheel prediction for the structure and orientation of KL_4 in a lipid environment; nevertheless, this lysine pattern was found to convey maximal surface activity [25]. A helical wheel projection of the KL_4 sequence assuming a canonical α-helical conformation reveals a side chain distribution that is at odds with partitioning of an amphipathic peptide within the plane of lipid bilayers in a membrane environment (Fig. 1A). Specifically, the canonical α-helical pitch does not produce a significant hydrophobic moment nor impart amphipathic characteristics to the peptide. The KL_4 sequence also does not contain a long enough hydrophobic segment to traverse the membrane, i.e. a transmembrane orientation of the peptide would bury 2–3 charged lysine side chains in the hydrophobic interior of the membrane. Previously, we have characterized the structure of KL_4 in POPC/POPG (3:1) lipid bilayers via solid state NMR spectroscopy and found that it adopts a structure that is helical yet more amphipathic than would be predicted by an α-helical conformation [20]. As depicted in Fig. 1B and C, structural models derived from NMR data of KL_4 in two different lipid environments exhibit a helical pitch of >4 residues/turn, in contrast to a canonical α-helix with 3.6 residues/ turn.

In order to more directly probe the insertion depth of KL_4 at the residue level, to characterize the effects of KL_4 on lipid dynamics on a nanosecond rather than microsecond timescale, and to determine the effects of KL_4 on solvent penetration into the lipid bilayers, we utilized site-directed spin labeling (SDSL) and EPR spectroscopy to examine the interaction of KL_4 with DPPC/POPG and POPC/POPG lipid vesicles. The use of power saturation experiments to generate a more quantitative, residue-specific partitioning profile for membrane-associated proteins is well-established [26], and yields information that is highly complimentary to our previous NMR studies [27,28]. By analyzing EPR line shapes and paramagnetic accessibility in a site-specific manner, we are developing a comprehensive model of the membrane bound orientation of KL_4, thus providing structural insights into its mechanism of action in restoring PS function and directing future rational development of more active SP-B peptidomimetics.

2. Materials & methods

2.1. Materials

POPC, DPPC, POPG, n-doxyl-PSPC (where $n = 5$, 7 and 12) and TEMPO-PC were purchased as chloroform solutions from Avanti Polar Lipids (Alabaster, AL) and quantified by phosphate analysis (Bioassay Systems, Hayward, CA). Iodoacetamido-PROXYL spin label (IAP) was purchased from Sigma (St. Louis, MO) and used as received. Unless otherwise stated, all other reagents were purchased from Fisher Scientific (Hampton, NH) and used as received.

2.2. Synthesis of KL_4

KL_4, (KLLLLKLLLLKLLLLKLLLLK) was synthesized via solid-phase peptide synthesis (ICBR Facility, UF), purified by RP-HPLC, and verified by mass spectrometry (m/z = 2469). Peptide was dissolved in methanol and analyzed by amino acid analysis for concentration (Molecular Structure Facility, UC Davis). Eight cysteine variants of KL_4, in which individual leucines were replaced by cysteine were also synthesized via solid-phase peptide synthesis (SPPS), purified, and mass verified (m/z = 2459).

2.3. Spin-labeling of KL_4 cysteine mutants

Cysteine containing KL_4 was dissolved in a minimal amount of King's reagent [29] and ether precipitated to ensure that the cysteine was reduced prior to spin labeling. The peptide was then dissolved at a concentration of ~0.1 mM in MeOH and KOH was added to adjust the pH to

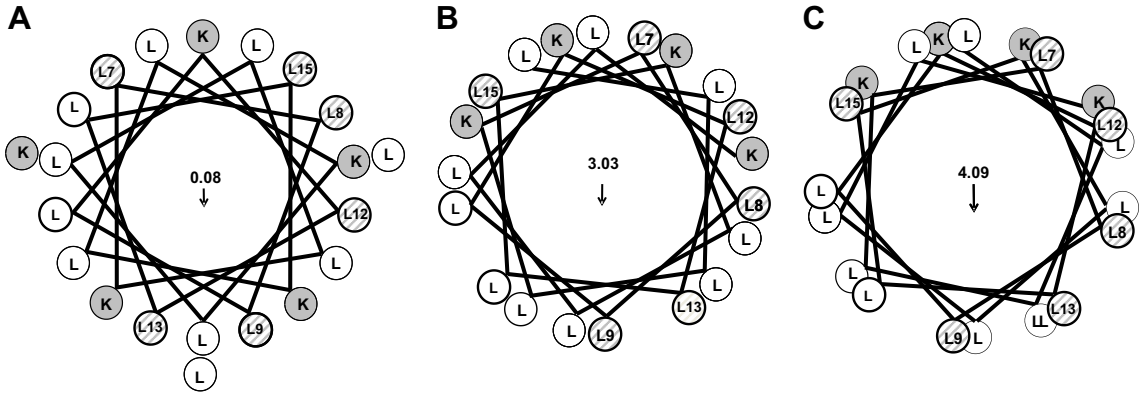

Fig. 1. Helical wheel plots of KL_4 with varying pitch. Wheels generated (A) assuming a canonical α-helix (3.6 residues/turn); (B) using the average torsion angles determined in POPC/POPG vesicles (4.1 residues/turn) [20]; and (C) using the average torsion angles suggested by preliminary NMR experiments with DPPC/POPG vesicles (4.6 residues/turn). Arrows indicate the net hydrophobic moments resulting from the distribution of charged lysine sidechains on the helix surface. The first lysine is not shown in (B) and (C) as NMR data indicate that the N-terminus is less structured relative to the rest of the helix. Leucines successively substituted with cysteine for SDSL-EPR experiments in this work are shown in gray crosshatch.

~7. A five-fold excess of tris(2-carboxyethyl)phosphine (TCEP) was added to keep the cysteine reduced. An appropriate volume of stock solution of 50 mM IAP spin label in DMSO was added to achieve a 20-fold excess of spin label to peptide. After being allowed to react in the dark for 4–5 h at room temperature, the spin-labeled peptide was purified via HPLC, and lyophilized fractions were solubilized in MeOH. The final peptide concentration for each spin-labeled sample was determined by either analytical HPLC or amino acid analysis (AAA).

2.4. Preparation of lipid/peptide samples

Lipid mixtures were prepared by mixing appropriate volumes of stock lipid chloroform solutions. For samples containing peptide, the peptide was added as a methanol solution to the lipid mixture in chloroform. Organic solvents were evaporated under nitrogen and the lipid films were re-suspended in warm cyclohexane (~45 °C), flash frozen and lyophilized. For each combination of lipids and peptide, two separate samples were prepared. The first was rehydrated with 140 mM NaCl, 10 mM Bis–Tris buffer, pH 6.5, and the second was rehydrated with 140 mM NaCl, 10 mM Bis–Tris buffer, pH 6.5, containing 10 mM NiAA (concentration adjusted and verified by UV–VIS absorption). The hydrated dispersions were subjected to >5 freeze–thaw cycles to form uniform MLVs and had 10 mM final lipid concentration of either 4:1 POPC/POPG or 4:1 DPPC/POPG. Samples containing spin-labeled lipid contained 1 mol% of either *n*-doxyl-PC (where $n = 5$, 7 and 12) or tempo-PC relative to the other lipids.

2.5. CD experiments

CD spectra were acquired at 45 °C on an Aviv Model 215 (Lakewood, NJ). Samples were prepared by hydrating lyophilized peptide–lipid powders in 10 mM Bis–Tris buffer, pH 6.5, with 140 mM NaCl, to achieve a final concentration of 35–50 μM KL_4, 2.5 mM lipids, and >5 freeze–thaw cycles were performed to form uniform MLVs, which were then extruded through 100 nm filters (Avanti Polar Lipids, Alabaster, AL) to form LUVs just prior to data collection. Data were background subtracted using buffer and lipid control samples.

2.6. CW-EPR spectroscopy

CW-EPR spectra were collected on a modified Bruker ER200 spectrometer (Billerica, MA) with an ER023M signal channel, an ER032M field control unit, and a loop gap resonator (Medical Advances, Milwaukee, WI). Spectra of samples containing either spin-labeled lipid or spin-labeled KL_4 were recorded at 45 °C. A quartz Dewar (Wilmad-Labglass, Vineland NF) surrounded the loop gap resonator for variable temperature experiments. Temperature was controlled by passing nitrogen gas through a copper coil submerged in a recirculating bath (Thermo Scientific) containing 40% ethylene glycol. For CW line shape analyses, typically a sample volume of 10 μL was utilized and spectra were collected using a 125 G sweep at a 2 mW power level, with 0.8–2 G modulation amplitude depending upon the inherent inhomogeneous line width. LabVIEW software (National Instruments, Austin, TX) was used for baseline correction and double integral area normalization using routines generously provided by Drs. Christian Altenbach and Wayne Hubbell (UCLA, Los Angeles, CA). Spectra were then analyzed for spin-label mobility in an empirical manner. These empirical line shape parameters include measuring the peak-to-peak line width of the central resonance line in the derivative spectrum, ΔH_{pp}, and the ratio of the central resonance intensity to the lower field intensity, $h_{(0)}/h_{(1)}$, as these parameters correlate with spin-label mobility and provide characterization of the local environment around the spin label [30–32].

2.7. Power saturation EPR experiments

EPR spectra were collected with parameters described above using gas-permeable TPX capillary tubes (Molecular Specialties Medical Advances, Milwaukee, WI) containing ~7–10 μL of sample that was equilibrated with either nitrogen gas or air (20% oxygen) until signal intensity no longer changed; typically around 15 min. The peak-to-peak first derivative amplitude, A_{pp}, of the central resonance ($h_{(0)}$) was measured and plotted as a function of microwave power, *P*, ranging in incident power from 0.2–63 mW. The resultant curves were fit to the expression:

$$App(0) = I\sqrt{P}\left[1 + \left(2^{-\varepsilon} - 1\right)\frac{P}{P_{1/2}}\right]^{-\varepsilon} \quad (1)$$

where *I* is a scaling factor, $P_{1/2}$ is the power at which the resonance amplitude is one-half its unsaturated value, and ε is a measure of homogeneity of the saturation of the resonance [26]. $P_{1/2}$ values were obtained under three conditions for all peptide/lipid samples:

1) Hydrated vesicles equilibrated under nitrogen gas, giving $P_{1/2}(N_2)$
2) Hydrated vesicles equilibrated under air (20% oxygen in compressed gas), giving $P_{1/2}(O_2)$
3) Hydrated vesicles equilibrated with 10 mM NiAA under nitrogen gas, giving $P_{1/2}$(NiAA).

No differences in line shape were noted on addition of NiAA or O_2, hence we did not need to account for ΔH_{pp} line width changes [33–35]. $\Delta P_{1/2}$ values were calculated by subtracting the $P_{1/2}(N_2)$ from either $P_{1/2}(O_2)$ or $P_{1/2}$(NiAA). A depth parameter, Φ, was calculated using the following formula:

$$\Phi = \ln\left[\Delta P_{1/2}(O_2)/\Delta P_{1/2}(\text{NiAA})\right] \quad (2)$$

3. Results

3.1. KL_4 secondary structure and spin labeling

Eight leucine positions in KL_4 (Fig. 1A) were individually replaced with cysteine and spin-labeled with IAP to allow analysis of the two hydrophobic segments at the center of the KL_4 sequence; allowing for the discrimination between a transmembrane or in-plane orientation of KL_4. IAP was utilized in these studies given that work from our lab on highly dynamic proteins has shown that the resulting S – S bond formed by the MTSL labeling of the CYS residue can be reduced, complicating CW data analysis due to the sharp signal from the released free spin-label as well as the possibility of dimerization of protein that can result from disulfide formation. Hence, given our past experiences [32], the IAP label was chosen. IAP is growing in popularity in the field given this potential problem of disulfide exchange when using MTSL labeling.

CD spectra (Supplementary Figure S1), and hence secondary structures, for six of the eight IAP-cysteine containing KL_4 constructs (L7P1, L8P1, L9P1, L12P1, L13P1 and L15P1; where P1 means the IAP modified CYS residue (Fig. 2) exhibited the same level of helicity as native KL_4 both in solution and in lipid environments. The EPR data for these six constructs are presented and are used for analyzing the partitioning of KL_4 into the lipid environments. For two of the constructs (L10P1 and L14P1) the CD spectra indicated a loss of helicity upon P1 incorporation; EPR data for these two constructs are provided in the Supplementary information (S2, S5), but these data were not used in developing the proposed model for KL_4 partitioning. Conventional CD fitting analyses reveal a significant degree of helical structure for both native KL_4 and spin-labeled (SL) KL_4 constructs when interacting with lipid LUVs.

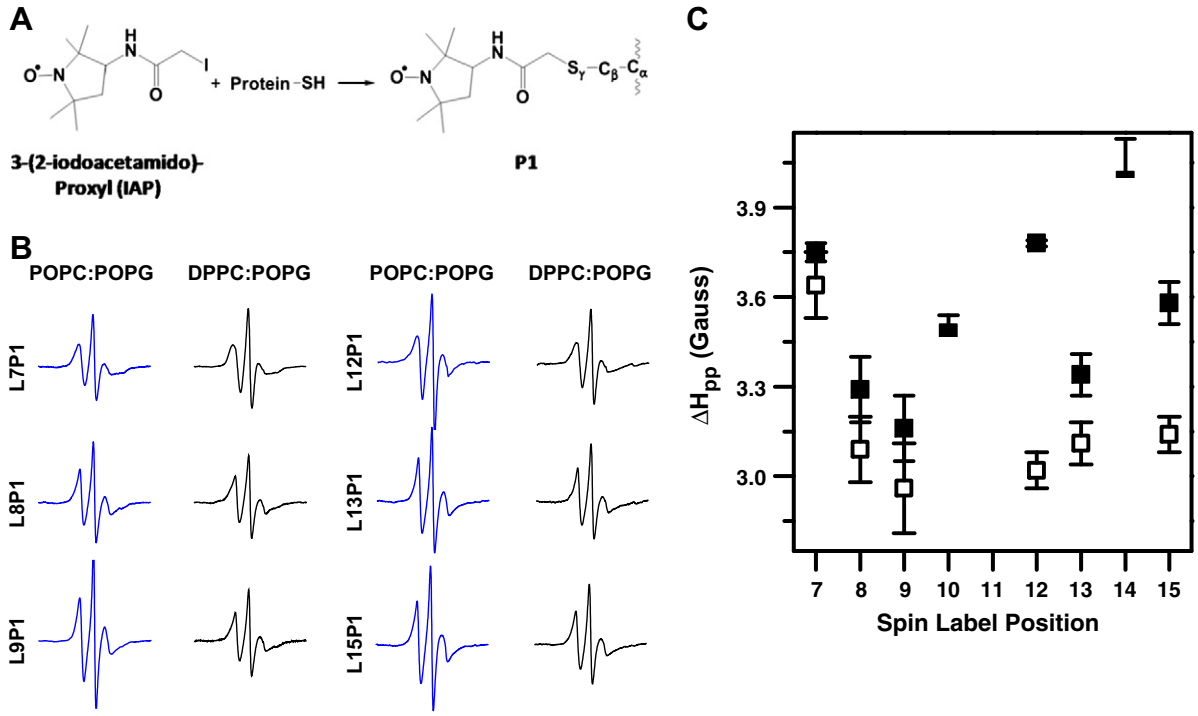

Fig. 2. (A) Scheme for attaching the IAP spin label to a cysteine residue via disulfide bond formation, producing a modified side chain referred to as P1. (B) 125 G X-band CW EPR spectra of KL_4-P1 variants reconstituted in lipid vesicles using a 50:1 L/P ratio. Data were collected at 45 °C and are displayed as double integral area-normalized spectra for easy comparison of spectral line shapes. (C) ΔH_{pp} for KL_4-P1 variants reconstituted in DPPC/POPG (solid squares) and POPC/POPG (open squares) lipid vesicles. Error bars represent the standard deviations determined from samples measured in triplicate, with the largest deviations occurring from fluctuations in temperature stability.

3.2. EPR line-shapes for SL-KL_4 support a surface bound orientation of the peptide

CW-EPR spectra of each SL-KL_4 peptide were collected for the peptide in methanol as well as interacting with the lipid systems of interest. Spectra obtained for the peptides in methanol have the expected fast limit nearly isotropic line shapes of small unfolded, soluble peptides (data not shown). Spectra collected in the presence of either DPPC/POPG or POPC/POPG are shown in Fig. 2. The mobility of each SL-KL_4 site upon partitioning into the two lipid systems was assessed by empirical line shape analysis. Specifically, ΔH_{pp} was measured as a function of spin-label position, and, for all sites investigated here, gave values ranging between 2.9 and 3.8 G ($\pm$0.1 G) for membrane bound KL_4 (Fig. 2B). The data shown were collected for a 50:1 L/P ratio, reflecting the composition of therapeutic Lucinactant which contains 2 mol% peptide relative to the lipids.

Inspection of these data supports two general results. First, spectra for all SL-KL_4 samples exhibit line shapes that are consistent with restricted motion reflective of membrane binding for non-aggregated helical proteins. The data in Fig. 2 are similar to those observed for interfacial orientations of single amphipathic sequences bound to membrane interfaces, such as α-synuclein [36], supporting an orientation of KL_4 parallel to the plane of the lipid bilayer. Additionally, the degree of mobility reflected in the motional averaging of the line shapes is uniformly higher than what has been observed for spin labels located in buried sites of soluble proteins, which exhibit spectra with central line widths of 5–8 G [37–39]. Taken together the X-band CW line shapes suggest that KL_4 is in a monomeric and not aggregated form. Second, for each site in SL-KL_4, the ΔH_{pp} values, which reflect the degree of motional averaging, differ in each lipid environment. Specifically, in DPPC/POPG lipid vesicles, the ΔH_{pp} value is consistently higher, indicating slower dynamics, than what is observed for the same position in POPC/POPG lipid vesicles. This result reveals that site-specific spin label mobility is dependent on the level of unsaturation in the phospholipids. This finding is in agreement with our previous NMR studies of lipid acyl chain dynamics and KL_4 leucine sidechain dynamics by ^{2}H NMR spectroscopy [27,28]. Mobility data from both NMR and SDSL indicate a deeper penetration of KL_4 in the more saturated lipid environment.

3.3. EPR line-shapes for n-doxyl lipids indicate that KL_4 increases local order in both DPPC/POPG and POPC/POPG lipid mixtures and penetrates more deeply into DPPC/POPG bilayers

For each lipid system, samples containing native KL_4 and spin-labeled lipids were analyzed to determine the effects of KL_4 on lipid mobility as a function of peptide concentration. Data were collected with liposome preparations that contain a final concentration of 1 mol% of *n*-doxyl-PSPC, where $n = 5, 7$, or 12, or 1 mol% TEMPO-PC relative to the bulk lipids (either 4:1 POPC/POPG or 4:1 DPPC/POPG). Empirical line shape parameters were determined to assess changes in mobility of the spin-label due to changes in the local environment. Shown in Fig. 3A are the relative percentage changes in ΔH_{pp}, calculated as $100 * (\Delta H_{pp(\text{with peptide})} - \Delta H_{pp(\text{without peptide})}) / \Delta H_{pp(\text{without peptide})}$, for 5-PCSL, 7-PCSL, and 12-PCSL incorporated into DPPC/POPG and POPC/POPG lipid mixtures as a function of KL_4 addition; no changes in ΔH_{pp} values for TEMPO-PC were observed on addition of KL_4 (data not shown). For both lipid systems, the relative percentage change in ΔH_{pp} at positions 5 and 7 is seen to increase upon addition of KL_4, consistent with a dose-dependent decrease in the mobility of the doxyl spin labels at these sites, revealing that the peptide is affecting the local environment at these positions and reducing motion of the lipids on the nanosecond timescale. At position 12, the DPPC/POPG system showed a dose-dependent decrease in mobility on addition of KL_4, whereas at this position in the bilayer, no changes in mobility were detected in the POPC/POPG system upon KL_4 addition. This result suggests again that KL_4 is partitioning more deeply into the DPPC/POPG bilayer and is able to interact with the 12-PCSL, whereas in the POPC/POPG bilayer the peptide partitions less deeply and thus does not affect mobility at

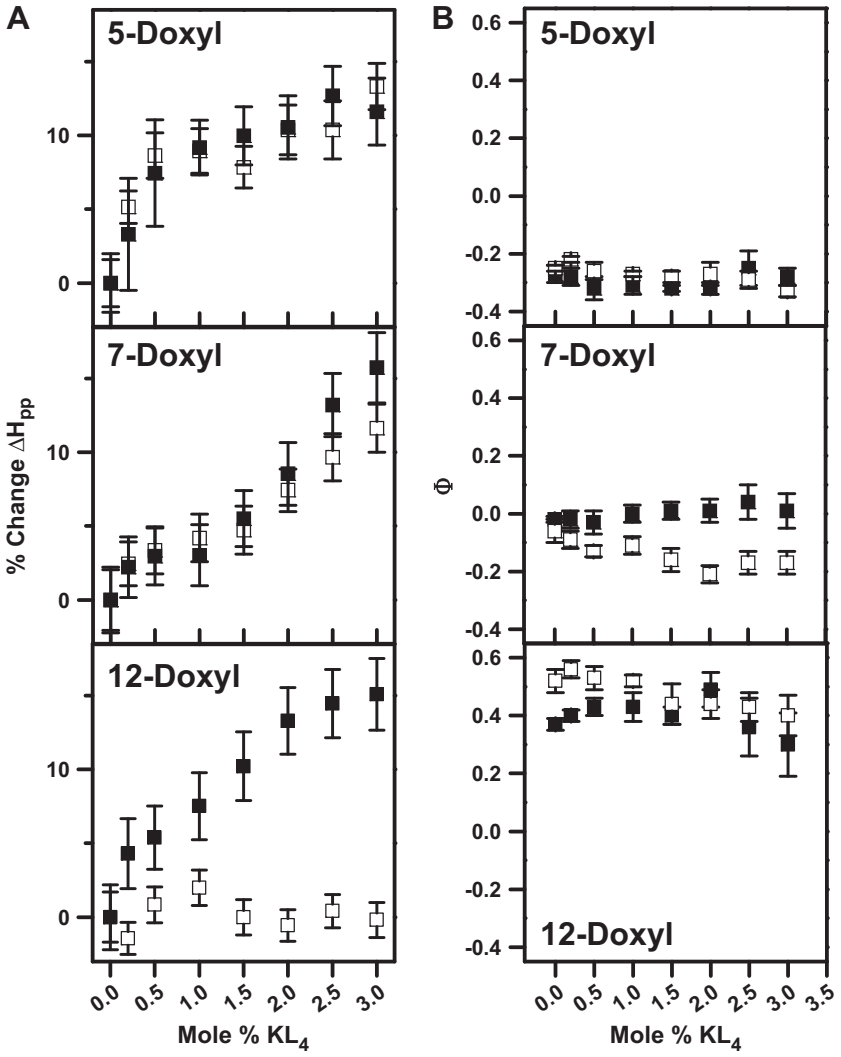

Fig. 3. Effects of KL_4 on lipid dynamics and spin-label accessibility measurements. Samples contain either 5-doxyl (top), 7-doxyl (middle), or 12-doxyl (bottom) in DPPC/POPG (solid squares) or POPC/POPG (open squares) lipid vesicles. (a) Relative percentage change of ΔH_{pp} for 5-PCSL, 7-PCSL, and 12-PCSL on partitioning of KL_4 into lipid vesicles at 45 ± 0.5 °C. Relative % change, calculated as $100 * (\Delta H_{pp(\text{with peptide})} - \Delta H_{pp(\text{without peptide})}) / \Delta H_{pp(\text{without peptide})}$, is plotted as the difference between ΔH_{pp} in the presence and absence of peptide for each doxyl-lipid. (b) Depth parameter, Φ, for the spin-labeled lipids in samples containing varying levels of KL_4, as measured by power saturation. Error bars represent the standard deviations determined from samples measured in triplicate on differing days. Errors arise primarily from temperature fluctuations. For ΔH_{pp} measurements 20 G scans were collected, providing better digital resolution.

the 12-PCSL position. Because the 12-doxyl line shapes are highly mobile approaching a fast limit X-band spectrum, further characterizations of mobility changes of the 12-doxyl spin label were made by calculating the ratio of the peak-to-peak amplitude of the central transition, $h_{(0)}$, and the low field transition, $h_{(1)}$ (Supplementary Figure S3). This parameter, $h_{(1)}/h_{(0)}$, has been shown to reflect conformational changes in unfolded highly dynamic proteins [31,32]. With this analysis, a small decrease in mobility can be detected in the POPC/POPG lipid environment, but it is substantially smaller than what is observed in DPPC/POPG lipid environment, providing further evidence that the penetration depth of KL_4 in these lipid systems is sensitive to the degree of lipid fatty acid saturation.

3.4. Power saturation measurements using n-doxyl lipids show decreased accessibility to both NiAA and O_2 with increasing KL_4, but the depth parameter Φ is unchanged

To calibrate relative O_2 and NiAA accessibility as a function of bilayer depth in the two lipid systems and to determine the effects of KL_4 on collisions of these paramagnetic species with *n*-doxyl lipids, we performed power saturation measurements on samples described above. For both lipid systems in the absence of peptide, it is noteworthy that Φ values for 5- and 7-doxyl are similar within error, and a slight difference in value is observed for 12-doxyl in these two systems (Fig. 3B). For both lipid systems, upon addition of KL_4, $\Delta P_{1/2}$ values decrease in a similar manner for both O_2 and NiAA at the 5-doxyl and 7-doxyl positions (Supplementary Figure S4). However, the results show that the relative frequency of collisions of NiAA at the 12-doxyl position in the different lipid systems is differentially altered upon KL_4 addition. For the POPC/POPG lipid mixture, the values decrease in a dose dependent manner; whereas for DPPC/POPG, values increase for higher KL_4 concentrations. On the other hand, while O_2 collisions decrease for both systems upon addition of KL4, the decrease is larger for the DPPC/POPG system. Together, these results provide additional evidence that KL_4 is likely partitioning further into the DPPC-rich bilayers. Shown in Fig. 3B are the calculated depth parameters, Φ, for the 5-, 7-, and 12-doxyl lipids as a function of KL_4 addition. Surprisingly, we find that the depth parameter, Φ, for the different spin labeled positions is minimally affected by

the addition of peptide, with only slight changes seen for the 7-doxyl and 12-doxyl positions in POPC/POPG bilayers. It appears that the relative changes in $\Delta P_{1/2}$ for both O_2 and NiAA as a function of KL_4 cancel one another out when taking the natural logarithm of their ratios. Caution should be made, however, that if Π (collision) values were to be reported, there would be differences. The presence of KL_4 changes both the apparent penetration of NiAA and O_2 in such a manner that the relative depth parameter is unaffected. Thus, the depth parameter value remains strongly correlated with lipid acyl chain position in both lipid systems, although the 5- and 7-doxyl positions have more similar depth parameters in the POPC/POPG bilayers, particularly after the addition of KL_4. These experiments serve as the necessary controls to calibrate a depth determination of SL-KL_4 described below. The fact that in the POPC/POPG system the 7-doxyl Φ value differs upon the addition of KL_4 demonstrates the need for the lipid values to be calibrated in an environment that contains a non-labeled protein when protein location (discussed below) is to be investigated.

3.5. Power saturation measurements on SL-KL_4 indicate that the peptide lies in the plane of the lipid bilayers and with a slightly altered helical structure to increase its amphipathic nature (hydrophobic moment); KL_4 penetration, helical pitch and orientation differ in the two lipid environments

Power saturation data for six KL_4-P1 variants partitioned into DPPC/POPG and POPC/POPG bilayers were collected with 2 mol% KL_4-P1 relative to the lipids (i.e. 50:1 L/P). A plot of Φ as a function of spin-label position in each of the lipid environments is shown in Fig. 4. For comparison, Φ values for the n-doxyl lipids at this peptide concentration are shown as dashed lines. For both lipid systems, four of the six sites are seen to partition to a depth range consistent with the locations of 5- and 7-doxyl SL lipids in the lipid acyl region. In both lipid systems, the periodic trends in Φ values are consistent with helices with periodicity >3.6 that lie perpendicular to the bilayer normal. Although the general structural features revealed by the power saturation measurements are similar in the two lipid systems, some noteworthy differences in the penetration depth and orientation of KL_4 as a function of lipid environment are observed.

The Φ values for sites 7, 8, and 9 are each larger in the DPPC system compared to the POPC system, indicating that this region is more deeply inserted in the DPPC/POPC lipid environment. For example, L7P1 is near the TEMPO position in POPC/POPG but near the 5-doxyl position in DPPC/POPG. In addition for L9P1 the Φ value is similar to that of 12-doxyl-PSPC in DPPC/POPG, whereas L9P1 is positioned between 7- and 12-doxyl in POPC/POPG. The trends in the Φ values for this region of KL_4 are consistent with the spin-label mobility parameter profiles in Fig. 2. For sites 12–15 the results indicate a consistent penetration level in both lipid systems with residues in the DPPC/POPG system located between the 5- and 7-doxyl positions and those in POPC/POPG having a depth slightly deeper than the 7-doxyl position, thus indicating a helix that tilts into the bilayer in the unsaturated lipids. For the DPPC/POPG system, results can be interpreted that the second half of KL_4 may kink back to the surface or, because the Φ values report on the location of the spin-label and not the protein backbone; this finding may indicate that the side-chains are snorkeling to the bilayer surface, which might be imposed by the closer packing of the saturated lipids. We feel that the second interpretation is more likely given that the spin-label mobility is more restricted compared to the unsaturated system (Fig. 2); again a possible signature of a snorkeling spin-label and consistent with the peptide partitioning very deeply into the lipid bilayers. This is in contrast to classical amphipathic helices, which

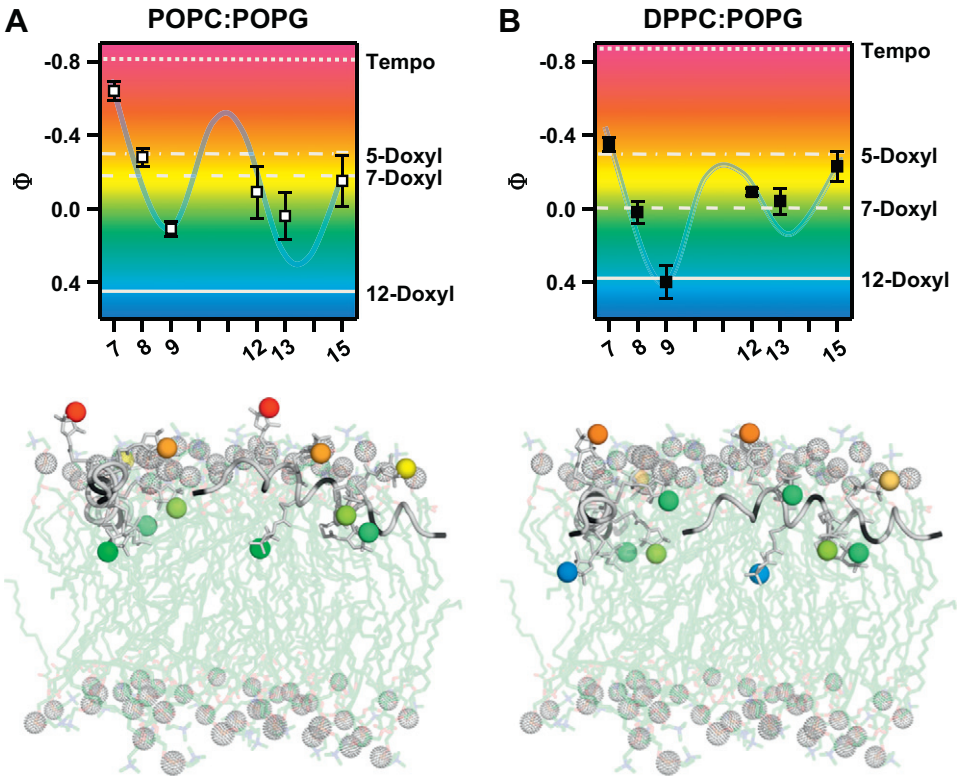

Fig. 4. (Top) Φ values for KL_4-P1 variants partitioning into (A) POPC/POPG and (B) DPPC/POPC. Data were collected for a 50:1 L/P ratio. Lines indicate Φ values obtained for spin-labeled lipids (indicated by tags) at equivalent L/P ratios. (Bottom) Models of KL_4 partitioning into (C) POPC-rich and (D) DPPC-rich regions. Partitioning depths are based on Φ values obtained for the KL_4-P1 constructs. The oxygens of the IAP N-O moieties used in this study are color-coded with respect to relative partitioning depth. The structural models for KL_4 are based on NMR measurements in POPC/POPG [20] and lipid coordinates are from model DPPC simulations [44]. Error bars represent the standard deviations determined from samples measured in triplicate on differing days. Errors arise primarily from temperature fluctuations.

contain a lower percentage of hydrophobic residues and which partition within the lipid headgroup region [36]. The overall pattern of the Φ values is consistent with the non-canonical helical wheel projections shown in Fig. 1B and C, with the resulting pattern indicative of KL_4 adopting an orientation that is parallel to the plane of the lipid bilayers.

Using a peptide model derived from ssNMR constraints [20] and the most likely conformers for IAP [40], models of KL_4 in the different lipid environments were developed to be consistent with the Φ values (Fig. 4); in these models, the oxygen in the N–O moiety is color coded to reflect the relative Φ value. Based on these models, we estimate that the center of the KL_4 helix is located 8–10 Å below the phosphates, considerably deeper than what has been observed for amphipathic helices which contain a more equal number of hydrophobic and hydrophilic residues [36].

4. Discussion

The dynamic nature of PS, with turnover of PS lipid stores every 5–10 h, requires rapid trafficking of lipids from tightly packed multilamellar structures to the monolayer at the air/fluid interface and likely differentiation of fully saturated DPPC from monounsaturated lipids and oxidized lipids. Lipid-rich PS relies on relatively low levels of lung surfactant proteins B (<0.2 mol%) to alter structure, dynamics, and phase properties of the lipids. Peptide mimics of SP-B, such as KL_4, are attractive in surfactant replacement therapy as they are more chemically uniform, less expensive and less immunologically reactive than exogenous lung extracts. A current formulation, Lucinactant, containing the KL_4 peptide was recently approved for the treatment of ARDS, but how this relatively simple peptide successfully restores lung compliance is not known.

Two conflicting models for KL_4 partitioning into lipid bilayers, either as a transmembrane helix or a helix lying in the plane of the bilayers, have been used to describe how KL_4 partitions into the lipid assemblies and modulates their properties. We have studied the dynamics of the lipids and several KL_4 leucine sidechains in POPC/POPG (3:1) and DPPC/POPG (4:1) environments via ^2H and ^{31}P NMR lineshape analyses [27,28]. Our findings are consistent with an in-plane orientation of KL_4 in the lipid bilayers, with deeper penetration occurring in DPPC:POPG (4:1) bilayers than in POPC/POPG (3:1) bilayer. An in-plane membrane bound orientation of KL_4 is also consistent with previous studies using peptides with hydrophobic/hydrophilic ratios similar to KL_4 which found that a transmembrane orientation is only favorable when the lysines are positioned closer to the N- and C-termini rather than throughout the peptide [41]. Our NMR studies also suggested that KL_4 penetrates much more deeply into the hydrophobic bilayer interior than typical amphipathic helices, particularly in DPPC-rich membranes. This is likely due to the higher hydrophobic residue content of KL_4, which contains only 24% charged/polar residues, relative to well-characterized amphipathic antimicrobial peptides, which generally contain ~50% charged/polar residues; a recent study of $SP\text{-}B_{63–78}$, part of the sequence from which KL_4 was developed, also shows significantly deeper peptide partitioning relative to typical amphipathic helices [42]. However, our NMR studies inferring the partitioning of KL_4 are based on measurements of lipid and peptide sidechain dynamics at a few select residues and do not yield a high-resolution, quantitative model of the orientation and partitioning depth of KL_4 into the lipid bilayers.

In this study we utilized EPR to more directly and quantitatively assay the partitioning depth of KL_4 into lipid environments and its effects on local lipid dynamics. To assay lipid specificity, we utilized two lipid systems: POPC/POPG, which is more typical of cell membranes, and DPPC/POPG, which is used in the clinical formulation of KL_4 and represents lipid species common in PS. We also chose temperature and pH conditions [43] similar to native PS and utilized peptide concentrations in the therapeutic range. Our results highlight both unique aspects of PS, stemming from the preponderance of DPPC, and the complexity of peptide/lipid interactions.

4.1. EPR measurements confirm that KL_4 peptide partitions in a planar orientation in fully hydrated lipid bilayers at physiologic temperature; partitioning depth is lipid dependent

The EPR line shapes and power saturation data for SL-KL_4 are in agreement with a lipid-dependent partitioning model. Importantly, the EPR data also point to an in-plane orientation of KL_4 in the lipid bilayers and a deeper penetration than is typically seen for amphipathic helical peptides, many of which are antimicrobial membrane-disrupting vehicles. The deeper penetration of KL_4 has been previously postulated and might play a critical role in its therapeutic activity. The deep penetration of the peptide as well as its sensitivity to lipid composition may also explain some of the discrepancies in interpreting previous low-resolution assays of KL_4 orientation in model membranes. A model for KL_4 partitioning and orientation in DPPC/POPG and POPC/POPG bilayers is presented in Fig. 4 with the relative side chain depths determined from our power saturation studies indicated. The peptide backbone is modeled based on NMR data for KL_4 in a POPC/POPG environment, with a helical pitch depicted in Fig. 1B. Superimposing most likely conformers of IAP [40] onto this structure leads to a model of peptide partitioning that is in very good agreement for the EPR measurements in POPC/POPG. The radial distribution of SDSL-KL_4 Φ values observed in the DPPC/POPG environment does not show a good agreement, suggesting that the structure of KL_4 may be slightly altered in the DPPC/POPG environment, with a higher helical pitch as depicted in Fig. 1C. Measurements via NMR of the structure of KL_4 in DPPC rich lipid bilayers are ongoing.

4.2. Differential partitioning of KL_4 into lipid bilayers leads to positive curvature strain for bilayers containing only monounsaturated lipids and stiffening of bilayers rich in DPPC

The SDSL lipid EPR line shapes collected in this study are sensitive to nsec timescale motions; comparing them to previous NMR work [27], which is sensitive to μsec timescale motions, allows us to distinguish between changes in collective (μsec) and local (nsec) motions. A direct comparison of EPR and ^2H NMR order parameter changes at the 5 and 12 acyl chain positions in these lipid systems is provided in the Supplementary information (S6). From the EPR line shapes, we are able to see a decrease in the local motion of the acyl chains at the 5, 7 and 12 positions in DPPC/POPG bilayers and at the 5 and 7 positions in POPC/POPG bilayers, consistent with KL_4 partitioning more deeply into DPPC/POPG lipid bilayers leading to increased local order further down the lipid acyl chains. In contrast, the ^2H NMR study showed decreased motional averaging in DPPC/POPG lipids and increased motional averaging in POPC/POPG lipids on addition of KL_4. Taken together, these observations lead to a model in which the addition of KL_4 increases collective (μsec) motions in the POPC/POPG lipid bilayers and decreases collective (μsec) motions in the DPPC/POPG lipid bilayers, yet also decreases local (nsec) motion in both environments, again consistent with different peptide partitioning depths between the two lipid bilayer systems. Changes in collective motions are also seen at a higher percentage of KL_4 than the changes in local motion (see Figure S6). These observations suggest that the addition of KL_4 leads to positive curvature strain in the POPC/POPG lipid system but stiffens the DPPC/POPG lipid bilayers.

5. Conclusion

Although KL_4 possesses an amphipathic peptide sequence that is helical in lipid bilayers, the relatively high percentage of leucine residues and unusual spacing of the lysine residues lead to a deeper average penetration depth than is typically seen for amphipathic helices. The peptide partitioning depth and orientation is sensitive to lipid acyl chain saturation. Deep penetration in the plane of the lipid bilayers likely leads to its sensitivity to lipid saturation and may underpin its

unique ability to serve as a therapeutic substitute for SP-B in PS replacement.

Acknowledgements

This research was funded by the Gates Foundation (J.R.L.), NIH R01 GM077232, NSF MCB 0746533, and NSF MCB 1239467 (G.E.F.). The assistance of Dr. Alfred Chung in peptide synthesis is gratefully acknowledged. The authors give special recognition to Dr. Frank Mills, who contributed greatly to the beginning of this work and passed away in 2011.

Appendix A. Supplementary data

Supplementary data to this article can be found online at http://dx.doi.org/10.1016/j.bbamem.2014.09.006.

References

[1] J. Goerke, Pulmonary surfactant: functions and molecular composition, BBA Mol. Basis Dis. 1408 (1998) 79–89.
[2] R.H. Notter, Lung Surfactants: Basic Science and Clinical Applications, vol. 149CRC Press, 2000.
[3] A.G. Serrano, J. Perez-Gil, Protein–lipid interactions and surface activity in the pulmonary surfactant system, Chem. Phys. Lipids 141 (2006) 105–118.
[4] J.C. Clark, S.E. Wert, C.J. Bachurski, M.T. Stahlman, B.R. Stripp, T.E. Weaver, J.A. Whitsett, Targeted disruption of the surfactant protein-B gene disrupts surfactant homeostasis, causing respiratory-failure in newborn mice, Proc. Natl. Acad. Sci. U. S. A. 92 (1995) 7794–7798.
[5] J.A. Clements, M.E. Avery, Lung surfactant and neonatal respiratory distress syndrome, Am. J. Respir. Crit. Care Med. 157 (1998) S59–S66.
[6] P.L. Ballard, J.D. Merrill, R.I. Godinez, M.H. Godinez, W.E. Truog, R.A. Ballard, Surfactant protein profile of pulmonary surfactant in premature infants, Am. J. Respir. Crit. Care Med. 168 (2003) 1123–1128.
[7] S.D. Revak, T.A. Merritt, E. Degryse, L. Stefani, M. Courtney, M. Hallman, C.G. Cochrane, Use of human surfactant low-molecular weight apoproteins in the reconstitution of surfactant biologic activity, J. Clin. Invest. 81 (1988) 826–833.
[8] B. Robertson, H.L. Halliday, Principles of surfactant replacement, BBA Mol. Basis Dis. 1408 (1998) 346–361.
[9] L.M. Nogee, G. Garnier, H.C. Dietz, L. Singer, A.M. Murphy, D.E. Demello, H.R. Colten, A mutation in the surfactant protein B gene responsible for fatal neonatal respiratory disease in multiple kindreds, J. Clin. Investig. 93 (1994) 1860–1863.
[10] A. Waring, W. Taeusch, R. Bruni, J. Amirkhanian, B. Fan, R. Stevens, J. Young, Synthetic amphipathic sequences of surfactant protein B mimic several physicochemical and in vivo properties of native pulmonary surfactant proteins, Pept. Res. 2 (1989) 308–313.
[11] S.D. Revak, T.A. Merritt, M. Hallman, G. Heldt, R.J. Lapolla, K. Hoey, R.A. Houghten, C. G. Cochrane, The use of synthetic peptides in the formation of biophysically and biologically-active pulmonary surfactants, Pediatr. Res. 29 (1991) 460–465.
[12] B. Robertson, J. Johansson, T. Curstedt, Synthetic surfactants to treat neonatal lung disease, Mol. Med. Today 6 (2000) 119–124.
[13] C.G. Cochrane, S.D. Revak, Pulmonary surfactant protein-B (Sp-B) — structure–function-relationships, Science 254 (1991) 566–568.
[14] C.G. Cochrane, S.D. Revak, A. Merritt, G.P. Heldt, M. Hallman, M.D. Cunningham, D. Easa, A. Pramanik, D.K. Edwards, M.S. Alberts, The efficacy and safety of KL(4)-surfactant in infants with respiratory distress syndrome, Am. J. Respir. Crit. Care Med. 153 (1996) 404–410.
[15] T.E. Wiswell, R.M. Smith, L.B. Katz, L. Mastroianni, D.Y. Wong, D. Willms, S. Heard, M. Wilson, R.D. Hite, A. Anzueto, S.D. Revak, C.G. Cochrane, Bronchopulmonary segmental lavage with Surfaxin (KL_4-surfactant) for acute respiratory distress syndrome, Am. J. Respir. Crit. Care Med. 160 (1999) 1188–1195.
[16] E. Piehl, A. Fernandez-Bustamante, Lucinactant for the treatment of respiratory distress syndrome in neonates, Drug Today 48 (2012) 587–593.
[17] F.R. Moya, J. Gadzinowski, E. Bancalari, V. Salinas, B. Kopelman, A. Bancalari, M.K. Kornacka, T.A. Merritt, R. Segal, C.J. Schaber, H. Tsai, J. Massaro, R. d'Agostino, A multicenter, randomized, masked, comparison trial of lucinactant, colfosceril palmitate, and beractant for the prevention of respiratory distress syndrome among very preterm infants, Pediatrics 115 (2005) 1018–1029.
[18] S.K. Sinha, T. Lacaze-Masmonteil, A.V.I. Soler, T.E. Wiswell, J. Gadzinowski, J. Hajdu, G. Bernstein, R. d'Agostino, A multicenter, randomized, controlled trial of lucinactant versus poractant alfa among very premature infants at high risk for respiratory distress syndrome, Pediatrics 115 (2005) 1030–1038.
[19] A. Saenz, O. Canadas, L.A. Bagatolli, M.E. Johnson, C. Casals, Physical properties and surface activity of surfactant-like membranes containing the cationic and hydrophobic peptide KL_4, FEBS J 273 (2006) 2515–2527.
[20] F.D. Mills, V.C. Antharam, O.K. Ganesh, D.W. Elliott, S.A. McNeill, J.R. Long, The helical structure of surfactant peptide KL_4 when bound to POPC: POPG lipid vesicles, Biochemistry 47 (2008) 8292–8300.
[21] M. Gustafsson, G. Vandenbussche, T. Curstedt, J.M. Ruysschaert, J. Johansson, The 21-residue surfactant peptide $(LysLeu_4)_4Lys(KL_4)$ is a transmembrane alpha-helix with a mixed nonpolar/polar surface, FEBS Lett. 384 (1996) 185–188.
[22] P. Cai, C.R. Flach, R. Mendelsohn, An infrared reflection–absorption spectroscopy study of the secondary structure in $(KL_4)_4K$, a therapeutic agent for respiratory distress syndrome, in aqueous monolayers with phospholipids, Biochemistry 42 (2003) 9446–9452.
[23] L.K. Tamm, S.A. Tatulian, Infrared spectroscopy of proteins and peptides in lipid bilayers, Q. Rev. Biophys. 30 (1997) 365–429.
[24] L. Martinez-Gil, J. Perez-Gil, I. Mingarro, The surfactant peptide KL_4 sequence is inserted with a transmembrane orientation into the endoplasmic reticulum membrane, Biophys. J. 95 (2008) L36–L38.
[25] G. Nilsson, M. Gustafsson, G. Vandenbussche, E. Veldhuizen, W.J. Griffiths, J. Sjovall, H.P. Haagsman, J.M. Ruysschaert, B. Robertson, T. Curstedt, J. Johansson, Synthetic peptide-containing surfactants — evaluation of transmembrane versus amphipathic helices and surfactant protein C poly-valyl to poly-leucyl substitution, Eur. J. Biochem. 255 (1998) 116–124.
[26] C. Altenbach, D.A. Greenhalgh, H.G. Khorana, W.L. Hubbell, A collision gradient-method to determine the immersion depth of nitroxides in lipid bilayers — application to spin-labeled mutants of bacteriorhodopsin, Proc. Natl. Acad. Sci. U. S. A. 91 (1994) 1667–1671.
[27] V.C. Antharam, D.W. Elliott, F.D. Mills, R.S. Farver, E. Sternin, J.R. Long, Penetration depth of surfactant peptide KL_4 into membranes is determined by fatty acid saturation, Biophys. J. 96 (2009) 4085–4098.
[28] J.R. Long, F.D. Mills, O.K. Ganesh, V.C. Antharam, R.S. Farver, Partitioning, dynamics, and orientation of lung surfactant peptide KL_4 in phospholipid bilayers, BBA Biomembranes 1798 (2010) 216–222.
[29] D.S. King, C.G. Fields, G.B. Fields, A cleavage method which minimizes side reactions following fmoc solid-phase peptide-synthesis, Int. J. Pept. Protein Res. 36 (1990) 255–266.
[30] G.E. Fanucci, D.S. Cafiso, Recent advances and applications of site-directed spin labeling, Curr. Opin Struct. Biol. 16 (2006) 644–653.
[31] B. Morin, J.M. Bourhis, V. Belle, M. Woudstra, F. Carriere, B. Guigliarelli, A. Fournel, S. Longhi, Assessing induced folding of an intrinsically disordered protein by site-directed spin-labeling electron paramagnetic resonance spectroscopy, J. Phys. Chem. B 110 (2006) 20596–20608.
[32] N.L. Pirman, E. Milshteyn, L. Galiano, J.C. Hewlett, G.E. Fanucci, Characterization of the disordered-to-alpha-helical transition of IA(3) by SDSL-EPR spectroscopy, Protein Sci. 20 (2011) 150–159.
[33] A.A. Frazier, M.A. Wisner, N.J. Malmberg, K.G. Victor, G.E. Fanucci, E.A. Nalefski, J.J. Falke, D.S. Cafiso, Membrane orientation and position of the C2 domain from cPLA2 by site-directed spin labeling, Biochemistry 41 (2002) 6282–6292.
[34] A.A. Frazier, C.R. Roller, J.J. Havelka, A. Hinderliter, D.S. Cafiso, Membrane-bound orientation and position of the synaptotagmin IC2A domain by site-directed spin labeling, Biochemistry 42 (2003) 96–105.
[35] J.D. Mathias, Y. Ran, J.D. Carter, G.E. Fanucci, Interactions of the GM2 activator protein with phosphatidylcholine bilayers: a site-directed spin-labeling power saturation study, Biophys. J. 97 (2009) 1436–1444.
[36] C.C. Jao, A. Der-Sarkissian, J. Chen, R. Langen, Structure of membrane-bound alpha-synuclein studied by site-directed spin labeling, Proc. Natl. Acad. Sci. U. S. A. 101 (2004) 8331–8336.
[37] H.S. Mchaourab, M.A. Lietzow, K. Hideg, W.L. Hubbell, Motion of spin-labeled side chains in T4 lysozyme, correlation with protein structure and dynamics, Biochemistry 35 (1996) 7692–7704.
[38] M. Margittai, D. Fasshauer, S. Pabst, R. Jahn, R. Langen, Homo- and heterooligomeric SNARE complexes studied by site-directed spin labeling, J. Biol. Chem. 276 (2001) 13169–13177.
[39] J.M. Isas, R. Langen, H.T. Haigler, W.L. Hubbell, Structure and dynamics of a helical hairpin and loop region in annexin 12: a site-directed spin labeling study, Biochemistry 41 (2002) 1464–1473.
[40] Y. Polyhach, E. Bordignon, G. Jeschke, Rotamer libraries of spin labelled cysteines for protein studies, Phys. Chem. Chem. Phys. 13 (2011) 2356–2366.
[41] B. Vogt, P. Ducarme, S. Schinzel, R. Brasseur, B. Bechinger, The topology of lysine-containing amphipathic peptides in bilayers by circular dichroism, solid-state NMR, and molecular modeling, Biophys. J. 79 (2000) 2644–2656.
[42] P. Bertani, V. Vidovic, T.C. Yang, J. Rendell, L.M. Gordon, A.J. Waring, B. Bechinger, V. Booth, Orientation and depth of surfactant protein B C-terminal helix in lung surfactant bilayers, BBA Biomembranes 1818 (2012) 1165–1172.
[43] R.M. Effros, F.P. Chinard, In vivo pH of extravascular space of lung, J. Clin. Invest. 48 (1969) 1983.
[44] S.E. Feller, R.M. Venable, R.W. Pastor, Computer simulation of a DPPC phospholipid bilayer: structural changes as a function of molecular surface area, Langmuir 13 (1997) 6555–6561.